Journal of Fluids and Structures (2000) **14,** 529–558
doi:10.1006/jfls.1999.0280, available online at http://www.idealibrary.com on IDEAL®

EXPERIMENTAL CHARACTERIZATION OF CENTRIFUGAL PUMPS AS AN ACOUSTIC SOURCE AT THE BLADE-PASSING FREQUENCY

G. Rzentkowski,

Atomic Energy Control Board, P. O. Box 1046, Station B, Ottawa, Ontario, K1P 5S9 Canada

AND

S. Zbroja

Ontario Hydro Technologies, Toronto, Ontario, Canada

(Received 15 April 1998, and in final form 8 November 1999)

Centrifugal pumps represent the primary source of acoustic energy in industrial piping. For hydraulically similar pumps, the amount of emitted energy may vary significantly between different designs and it is generally not known. The available information, typically presented as a magnitude of pressure pulsations measured at the pump discharge, is not free of resonance effects associated with the piping acoustics and, in some aspects, may be seriously misleading. In this paper, we formulate an experimental method to examine the pump acoustic characteristics at the blade-passing frequency. First, we assess the resonance effects in the test-loop. Next, we decompose the measured signal into the components associated with the pump action and with the loop acoustics by means of a simple pump model which is based on a linear superposition of pressure wave transmission and excitation. We apply this technique to examine the acoustics of a single-stage, double-volute centrifugal pump. We estimate the strength of source variables and establish the pump characteristics as an acoustic source. The results indicate that (i) the source variables represent a jump in the acoustic field and are nearly free of resonance effects in the test-loop and that (ii) the pump may act either as a pressure or as a velocity source. Based on this analysis, we postulate that the pressure wave traveling in the direction of pump discharge should be used to define the pump pulsation level for valid comparison between different designs and for acoustic modelling of piping systems. © 2000 Academic Press

1. INTRODUCTION

The prediction of flow-induced vibration in fluid-filled industrial piping may require the exact knowledge of the system acoustics, the means by which pressure pulsations are generated and transmitted. These pulsations, propagating away from a source in the form of acoustic waves, can be reflected by the system discontinuities (side branches, changes in cross-section, entrances to volumes, etc.) forming standing waves. Standing waves may strongly interact with a piping system or its elements, leading to excessive vibration and alternating stresses beyond endurance limits. Several cases of this nature were reported, especially in chemical, petro-chemical and power generation industries, causing costly repairs and loss of power. The most recent example is fuel bundle damage and excessive pressure tube fretting observed at the start-up of CANDU (Canada Deuterium Uranium) reactors constructed in Darlington, Canada (Rzentkowski *et al.* 1993). This incident had severe safety and economical implications, and indicated that a better knowledge of piping acoustics, including the acoustic characteristics of excitation sources, is required to enable

0889–9746/00/050529 + 30 $35.00/0 © 2000 Academic Press

the designer, at least in principle, to address the problem of acoustic resonance on the drawing board.

The primary sources of pressure generation in fluid-filled industrial piping are typically centrifugal pumps. The acoustic energy is mainly radiated as a result of turbulence and a discrete excitation at the blade-passing frequency. Very little is known about excitation sources within pumps except to say that a hydraulically well-designed pump generates lower dynamic pulsations. The amount of emitted energy may vary significantly between different pump designs. It depends on the pump size and speed, and on the design details of the impeller and cutwater [see, for example, the review papers of Guelich & Bolleter (1992) and Rzentkowski (1996)]. Despite some experimental and analytical efforts, leading to a better understanding of pumps as an acoustic source, most pump suppliers either do not have or do not provide this information. The predictive tools (Simpson *et al.* 1967; Guelich & Bolleter 1992), on the other hand, cannot be universally applied. They rely exclusively on statistical correlations that involve the pump size and speed, lacking the details of the impeller and cutwater geometry. Another complicating factor is the fact that the available information from laboratory tests and field measurements is not free of resonance effects associated with the piping system acoustics. Thus, this information is not exclusively related to the base pulsation level (source strength) emitted by pumps, which should be used for valid comparison between different designs. Also, the scaling effect between pumps of different size and speed has not yet been determined. For practical purposes, a square law between pressure pulsations and circumferential impeller velocity is used (Guelich & Bolleter 1992), implying that centrifugal pumps act exclusively as a pressure source, which is equivalent to an acoustic dipole in a piping system. This assumption, however, contradicts the recent findings of experimental studies on unsteady velocity distribution within centrifugal pumps. Several flow structures, all directly related to the blade–tongue interaction and to the nonuniform out-flow from the impeller, have been identified [see, for example, de Jong *et al.* (1993) and Chu *et al.* (1993)]. While the first represents an acoustic dipole, the latter can cause the incidence of an acoustic monopole source characterized by a net mass flow out of a source. All the aforementioned points, regarding the measurement and reporting of pump-generated pressure pulsations, are critical. They lead to the conclusion that the available information is incomplete and, in some aspects, may be seriously misleading.

In our earlier study (Rzentkowski & Zbroja 1997), we formulated an experimental method to examine the pump acoustic characteristics and to report the test data. First, we assessed the resonance effect in a test loop by calculating the reflection coefficient at the pump ports, based on a two-sensor method. Next, we decomposed the measured signal into the components associated with pump action (source pressure and velocity) and loop acoustics with the use of a simple pump model. We formulated a pump model based on a transmission matrix approach, without exploring the flow excitation mechanisms and without detailed modelling of the flow passages within the pump volute and impeller. In this way, we obtained the net source pressure and velocity as a jump in the acoustic field at the pump discharge port where the excitation source was assumed. We applied this approximate analysis over a wide range of temperatures (acoustic wavelengths) to assess the acoustic characteristics of a single-stage, double-volute CANDU heat transport pump. We found that the predictions were sensitive to the physical location of the pump ports. We were thus not able to completely isolate the pump action from the acoustic effects in the test-loop.

In the present study, we refine this experimental identification procedure. We apply a multi-sensor technique, which is less sensitive to transducer spacing and random measurement errors, to assess resonance effects in the test-loop. We also improve the pump model with the use of a scattering matrix approach, which is better suited for distributed systems.

That is, we examine a local pressure field in the pump vicinity by considering travelling waves. For a straight section of suction and discharge piping, this approach is not sensitive to the physical location of the pump ports. We thus postulate that the amplitude of pressure waves travelling in the direction of pump discharge should be used in experimental situations to define the base pulsation level emitted by pumps. We apply this method to the CANDU heat transport pump, which has been already examined in our earlier study (Rzentkowski & Zbroja 1997), and compare the model's predictions with the results of transmission matrix calculation. We also attempt to extrapolate the source variables from the discharge port to the pump cutwaters, which are assumed here to represent the primary source of acoustic excitation at the blade-passing frequency. In this way, we demonstrate that the pump source variables are nearly free of acoustic resonance effects in the test loop and that the pump may act either as a pressure or as a velocity source.

2. FORMULATION OF EXPERIMENTAL TECHNIQUE

In this section, we formulate an experimental technique for acoustic analysis of centrifugal pumps at the blade-passing frequency. First, we assess the resonance effect in the test loop. Next, we decompose the measured signal into the components associated with pump action and loop acoustics. For this, we assume that:

(i) the general pressure field in a piping system is one-dimensional and, due to the reflective characteristics of a piping system, can be expressed as superposition of two waves travelling in opposite directions;
(ii) the general pressure field in the pump vicinity represents a linear superposition of wave transmission through a pump and excitation of source variables (source variables introduce a jump in the acoustic field at the pump discharge port);
(iii) the description of pump geometry is reduced to a "black box" but accounts for coupling between the field variables at the pump suction and discharge ports (the suction and discharge flanges are chosen as the pump ports);
(iv) the source variables at the pump ports are modelled as acoustic pressure and velocity without exploring the underlying flow excitation mechanisms; and
(v) the pump transmission characteristics are modelled with the use of approximate empirical expressions.

The analysis technique advanced in this paper is conceptually identical to that formulated in our previous study (Rzentkowski & Zbroja 1997). It differs only in some specific details of the loop and pump acoustic modelling.

2.1. Test Loop Acoustics

2.1.1. *Pressure field decomposition*

Consider a uniform piping element, as shown in Figure 1. Due to reflective characteristics of the piping system, the general one-dimensional pressure field represents a superposition of two waves travelling in opposite directions (Morse & Ingard 1986; Davis 1988),

$$p(x, t) = p^+(x, t) + p^-(x, t), \tag{1}$$

while the resultant velocity field is

$$q(x, t) = \frac{1}{\rho c}\,[p^+(x, t) - p^-(x, t)], \tag{2}$$

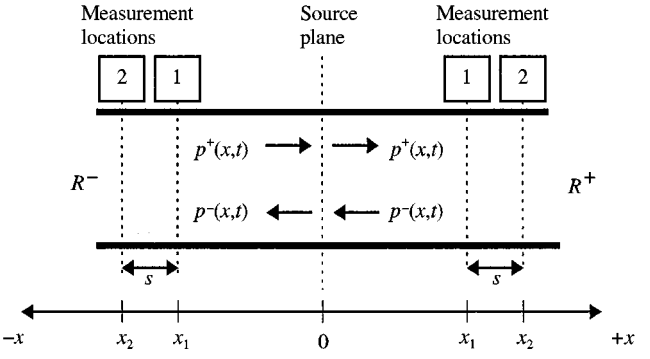

Figure 1. Representation of acoustic pressure field in a piping system element using a superposition principle.

where $p^+(x, t)$ and $p^-(x, t)$ denote, respectively, pressure waves travelling in the direction of x positive and negative, ρ is the fluid density and c is the speed of sound.

As shown by Chung and Blaser (1980a, b), both wave components can experimentally be determined from pressure measurements at two locations separated by the distance s along a uniform piping element. Namely,

$$p^+(x, \omega) = \frac{1}{e^{jks} - e^{-jks}}(p_1 e^{jks} - p_2) \tag{3}$$

and

$$p^-(x, \omega) = \frac{1}{e^{jks} - e^{-jks}}(-p_1 e^{-jks} + p_2), \tag{4}$$

where p_1 and p_2 represent measurements at locations x_1 and x_2, respectively, ω is the frequency of pressure pulsations, $k = \omega/c$ is the wavenumber (neglecting wave attenuation), and $j = \sqrt{-1}$ is the complex number. As denoted in Figure 1, equations (3) and (4) apply directly to the directions of x positive and negative.

Although the dynamic pressure can easily be measured, the results of pressure field decomposition are very sensitive to the transducer spacing (the method has a spectrum of singular points for multiples of the wavenumber, $f_n = nc/2s$ where $n = 1, 2, 3 \ldots$), and measurement errors introduced by instrumentation or random pressure field disturbances. The decomposition accuracy may be improved with the use of more than two pressure transducers, since with each additional transducer two more equations are added to the system description (waves travelling in opposite directions). In this way, equations (3) and (4) become overdetermined and the solution may be obtained in the form of a least-square-fit approximation. Nevertheless, in the neighbourhood of singular points, a large error in the pressure field decomposition may be expected, imposing some restrictions on the application of equations (3) and (4) to experimental situations.

Here, we recommend an alternative approach (Edge & Johnston 1990) which requires at least three measurement points in a uniform section of pipe and is less sensitive to the transducer spacing. By considering a standing wave pattern in a piping system, we can rewrite equation (1) as

$$p(x, \omega) = p^+(0)e^{-jkx} + p^-(0)e^{jkx}, \tag{5}$$

where $p^+(0)$ and $p^-(0)$ represent the complex amplitudes at the origin, $x = 0$, of the waves traveling in opposite directions (see Figure 1). They can be expressed as

$$p^+(0) = c_1 + \mathrm{j}c_2 \tag{6}$$

and

$$p^-(0) = c_3 + \mathrm{j}c_4, \tag{7}$$

where the wave coefficients c_1, c_2, c_3, and c_4 are real numbers. Once these coefficients are known, the wave amplitudes, and thus the pressure field, can fully be characterized at any location along a uniform section of a piping system. To find these coefficients, we use the system identification procedure that is based on a least-square-error fit between the measured and predicted pressure (Edge & Johnston 1990). This procedure yields an optimum set of the wave coefficients c_1, c_2, c_3, and c_4. It must be appreciated that the residual error may still be present, especially if the one-dimensional pressure field assumption is not fully satisfied in the measurement locations or the speed of sound is not known exactly.

To minimize the residual error in equations (6) and (7), we develop here an experimental procedure for a qualitative assessment of pressure measurements. We introduce the reflection coefficient as the ratio between the reflected and incident waves amplitudes, $R = p^-(0)/p^+(0)$, and rewrite equation (5) in the following form:

$$p(x, \omega) = p^+(0)(\mathrm{e}^{-\mathrm{j}kx} + R\mathrm{e}^{\mathrm{j}kx}). \tag{8}$$

After some algebra (details are given in Appendix B), it can be shown that the acoustic pressure field forms an ellipse when plotted in a complex form, namely

$$\left[\frac{X}{p^+(0) \quad (1+r)}\right]^2 + \left[\frac{Y}{p^+(0) \quad (1-r)}\right]^2 = 1, \tag{9}$$

where $r = R/\mathrm{e}^{2\delta}$ (δ is an angle of ellipse rotation relative to the reference coordinate system), and X and Y represent, respectively, the real and imaginary parts of the acoustic pressure. Thus, for pressure measurements conducted in a uniform section of pipe, any deviation from this equation may be attributed to measurement errors. It thus follows that equation (9) provides a very convenient tool to assess if the measured pressure agrees with the assumption of one-dimensional wave propagation.

The speed of sound, required to calculate the wavenumber in equations (6) and (7), can theoretically be determined from fluid properties and elastic deformation of the pipe walls [see, for example, Chaudhry (1986)]. Direct measurements, however, are preferable to eliminate uncertainties related to system conditions (e.g., temperature and pressure) and piping vibration. Here, we use the system identification procedure previously formulated to solve equations (6) and (7). First, we find the complex wave amplitude for an assumed speed of sound and compare it against measurements. The residual error reflects discrepancy between the assumed and the actual speed of sound if we neglect small measurement noise distorting the pressure field. Next, we minimize this error by independently varying the speed of sound for a given system temperature.

2.1.2. *Acoustic impedance and reflection coefficient at the pump ports*

At any arbitrary location in a piping system, the ratio between the acoustic pressure and velocity, equations (1) and (2), determines the acoustic impedance, and the ratio between the reflected and incident waves, equations (3) and (4), determines the reflection coefficient. Both

are complex whenever a reflected wave is present. The magnitude of an acoustic impedance may vary between zero and infinity. It is typically normalized by the impedance of an infinite pipe which is equal to ρc. The magnitude of the reflection coefficient represents the amount of reflected energy; it reaches a maximum of one for a fully reflective termination and a minimum of zero for a nonreflective termination.

For a piping element shown in Figure 1, the normalized acoustic impedance, Z, and the reflection coefficient, R, at location x_2, in the direction of x positive and negative, can be written in the following forms (Chung & Blaser 1980a, b), respectively,

$$Z = \frac{1 + e^{jks} - H_{21}(1 + e^{-jks})}{1 - e^{jks} + H_{21}(1 - e^{-jks})} \tag{10}$$

and

$$R = \frac{e^{jks} - H_{21}}{1 - H_{21}e^{-jks}}, \tag{11}$$

where H_{21} is the complex transfer function between pressure at both measurement locations. We can rearrange equations (10) and (11) to find a direct relationship between the acoustic impedance and the reflection coefficient. This yields $Z = (1 + R)/(1 - R)$, meaning that for a nonreflective termination, $R = 0$, the magnitude of the normalized impedance is equal to one, $Z = 1$.

2.2. Pump Model

Centrifugal pumps can be modelled to a various degree of complexity without exploring the underlying flow excitation mechanisms. In most practical applications, the description of pump geometry is reduced to a "black box" with single or two ports (typically, the suction and discharge flanges are chosen as the pump ports). The one-port model is directly applicable to positive-displacement pumps and multi-stage centrifugal pumps that do not have a clear flow path between the suction and discharge ports; i.e., there is limited acoustic transmission between the two ports, and the model describes the relationship between acoustic pressure and velocity at the discharge port, independent of the condition at the suction port. The acoustic transmission is also restricted at higher frequencies for which the acoustic wavelength approaches the pump diameter. It is thus reasonable to expect that there is a frequency threshold above which the one-port model is applicable to any centrifugal pump (Whitson & Benson 1993, Bolleter 1993). The two-port model represents a more general description of centrifugal pumps, allowing for the transmission of acoustic waves between pump ports. Thus, its application is not restricted by the pump geometry and size, and the acoustic wavelength. The pump transmission characteristics, however, are not known in general and direct measurements for every pump type are needed by subjecting the pump to externally generated pressure pulsations and by measuring the system response at various points along the discharge and suction. Practical application of these techniques to large pumps, which require suppression of pump noise by an external source, is very difficult. As we discuss later, in the absence of direct measurements, approximate empirical expressions can be used to represent the pump transmission characteristics.

2.2.1. *One-port model*

The one-port source represents the simplest acoustic model of a pump; it is assumed that there is no coupling between the field variables at the pump suction and discharge. The

pump is thus characterized by the excitation of source variables only and may be exclusively described by the source strength, p_s and the source impedance, Z_s, which in this case is equivalent to the pump impedance (the resultant source velocity is $q_o = p_s/Z_s$). For the one-port pump representation, the acoustic pressure at the port positioned at the measurement location is given by (De Jong *et al.* 1993)

$$p_o = p_s\left(\frac{Z_o}{Z_s + Z_o}\right), \tag{12}$$

and consequently the acoustic velocity can be expressed as

$$q_o = p_s\left(\frac{1}{Z_s + Z_o}\right), \tag{13}$$

where Z_o denotes the system impedance at the pump port, either discharge or suction, which can experimentally be determined from equation (10). It is evident from equations (12) and (13) that the field variables at the pump port depend on the piping system acoustic characteristics. Note, however, that if $Z_s \ll Z_o$ the acoustic pressure at the port is independent of the system impedance, $p_o = p_s$ (constant pressure source), whereas if $Z_s \gg Z_o$ the acoustic velocity at the port is independent of the system impedance, $q_o = p_s/Z_s$ (constant velocity source). It thus follows that only the constant pressure and the constant velocity sources may give an exact measure of the source strength without determining the piping system acoustics.

It is worth noting that, for the one-port pump representation, the description of the pressure and velocity sources is equivalent. This is an important point, meaning that two different sources can have an identical pressure field. Therefore, source characteristics cannot be uniquely determined from the pressure field measurements in the pump vicinity.

2.2.2. *Two-port model*

The two-port source represents a more accurate model of a centrifugal pump; it accounts for coupling between the field variables at the pump suction and discharge ports. The source is thus characterized by the transmission of pressure waves through the pump (passive element) and the excitation of source variables (active element). Here, for simplicity, we assume that a single-point source, which introduces a jump in the acoustic field, is positioned at the pump discharge port. The field variables at the pump ports can be expressed either in terms of acoustic pressure and velocity or, alternatively, in terms of acoustic pressure waves travelling in opposite directions. The first approach yields the solution of the acoustic pressure field in a transmission matrix form while the second in a scattering matrix form.

With the use of a transmission matrix representation, the source pressure, p_s, and velocity, q_s, at the pump ports can be related as (Stirnemann, 1987)

$$\begin{Bmatrix} p_o \\ q_o \end{Bmatrix} = \begin{bmatrix} T_{11} & T_{12} \\ T_{21} & T_{22} \end{bmatrix} \begin{Bmatrix} p_i \\ q_i \end{Bmatrix} + \begin{Bmatrix} p_s \\ q_s \end{Bmatrix}, \tag{14}$$

where the subscripts 'o' and 'i' refer to the pump discharge and suction field variables, respectively, and T_{ij} are the transmission matrix elements. Equation (14) is sufficient to describe the local pressure field in the pump vicinity if the pump ports are positioned at the measurement location. Otherwise, equation (14) must be modified to

include acoustic properties of a piping element between the measurement points and the pump ports.

It can be seen that equation (14) represents a linear superposition of the wave transmission and excitation. This implies that the source variables at the pump port are independent of the piping system acoustics (it must be realized, however, that the piping system acoustics may eventually alter the noise generation mechanism and thus may change the magnitude of the source variables). The field variables, on the other hand, depend not only on the source variables and the pump transmission characteristics but also, as in the case of one-port model, on the pump port impedance. To demonstrate this point, and yet make the analysis as simple as possible, we assume here that the acoustic source represents a source plane [i.e., $T_{12} = 0$ and $T_{21} = 0$ in equation (14)] characterized by a discontinuity in the local acoustic field: either velocity for a velocity source or pressure for a pressure source. Equation (14) thus becomes $p_o = p_i$ and $q_o = q_i + q_s$ for a velocity source, and $p_o = p_i + p_s$ and $q_o = q_i$ for a pressure source. Substituting $p_o = q_o Z_o$ and $p_i = q_i Z_i$ in the first set of equations, and $q_o = p_o/Z_o$ and $q_i = p_i/Z_i$ in the second set, we may now show that if $Z_i \ll Z_o$ the acoustic pressure at the port is independent of the system impedance, $p_o = 0$ for a velocity source and $p_o = p_s$ for a pressure source (constant pressure source), whereas if $Z_i \gg Z_o$ the acoustic velocity at the port is independent of the system impedance, $q_o = q_s$ for a velocity source (constant velocity source) and $q_o = 0$ for a pressure source.

Note that with the use of equation (14) we may directly determine the source characteristics from the pressure field measurements local to the pump by assuming, respectively, $q_s = 0$ and $T_{21} = 0$ for a pressure source (no jump in the acoustic velocity, $q_o = q_i$), and $p_s = 0$ and $T_{12} = 0$ for a velocity source (no jump in the acoustic pressure, $p_o = p_i$). In this way, we may exclusively relate a jump in the acoustic field to the excitation of source variables by the pump and determine the acoustic nature of a source (pressure versus velocity). It must be realized, however, that equation (14) gives the exact description of the source variables and the pump acoustic characteristics if the pump is acoustically equivalent to a point or a plane source; i.e., if flow passages within the pump are significantly shorter than acoustic waves. Otherwise, the source pressure and velocity may assume a range of values, depending on the physical model chosen to represent the pump geometry, or specifically, depending on the location of pump ports (de Jong 1994). It thus follows that equation (14), although it provides an approximate measure of the source strength, cannot be used with confidence to determine the relative magnitudes of source variables and to determine the source characteristics for large pumps. This requires a more detailed modelling of the flow passages and acoustic sources within the pump volute.

Based on the transmission matrix formulation, centrifugal pumps can be modelled to various degrees of complexity. Some examples of more complex pump models, yet sufficiently simple for engineering applications, are shown in Table 1. Interestingly, whichever pump representation used, the pump transmission and excitation characteristics can always be reduced to the basic form of equation (14). This, however, requires understanding of the noise generation mechanisms which, in general, are not known precisely due to the flow complexity within the pump volute. Also, as we discuss later, many excitation mechanisms can exist simultaneously, making detailed modelling attempts rather difficult.

Here, we recommend an alternative approach with the use of the scattering matrix representation that gives a more convenient description of the acoustic source within a piping system without exploring the underlying noise generation mechanisms. The acoustic source and pressure field are expressed in terms of the waves travelling in opposite directions and thus remain constant in a straight section of a piping system adjacent to the pump (see Figure 1). The transmission equation, equivalent to equation (14),

TABLE 1

Simplified transmission matrix models of centrifugal pumps reduced to the basic form of equation (14)

Model description	Pump schematics	Pump matrix	Source vector
Source at the pump discharge port: equation (14)	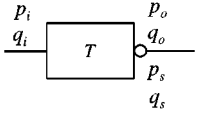	$[T]$	$\begin{pmatrix} p_s \\ q_s \end{pmatrix}$
Source within pump ports	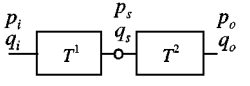	$[T] = [T^2][T^1]$	$[T^2]\begin{pmatrix} p_s \\ q_s \end{pmatrix}$
Source at a branching element boundary within pump ports	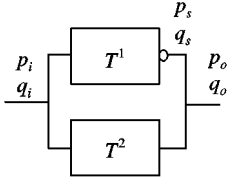	$T_{11} = \dfrac{T^1_{11}T^2_{12} + T^1_{12}T^2_{11}}{T^1_{12} + T^2_{12}}$ $T_{12} = \dfrac{T^1_{12}T^2_{12}}{T^1_{12} + T^2_{12}}$ $T_{21} = \dfrac{(T^1_{22} - T^2_{22})(T^2_{11} - T^1_{11})}{T^1_{12} + T^2_{12}} + T^1_{21} + T^1_{21}$ $T_{22} = \dfrac{(T^1_{22}T^2_{12} + T^2_{22}T^1_{12})}{T^1_{12} + T^2_{12}}$	$\begin{bmatrix} \dfrac{T^2_{12}}{T^1_{12} + T^2_{12}} & 0 \\ \dfrac{T^2_{22} + T^1_{22}}{T^1_{12} + T^2_{12}} & 1 \end{bmatrix}\begin{pmatrix} p_s \\ q_s \end{pmatrix}$
Multiple, synchronized sources within pump ports	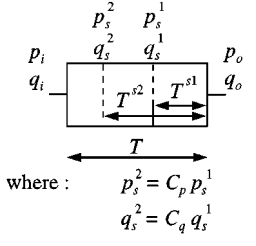	$[T]$	$\begin{bmatrix} T^{S1}_{11} + C_p T^{S2}_{11} & T^{S1}_{12} + C_q T^{S2}_{12} \\ T^{S1}_{21} + C_p T^{S2}_{21} & T^{S1}_{22} + C_q T^{S2}_{22} \end{bmatrix}\begin{pmatrix} p_s \\ q_s \end{pmatrix}$
Multiple, synchronized sources at the element boundaries within pump ports.	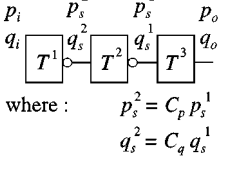	$[T^3][T^2][T^1]$	$\begin{bmatrix} T^{S1}_{11} + C_p T^{S2}_{11} & T^{S1}_{12} + C_q T^{S2}_{12} \\ T^{S1}_{21} + C_p T^{S2}_{21} & T^{S1}_{22} + C_q T^{S2}_{22} \end{bmatrix}\begin{pmatrix} p_s \\ q_s \end{pmatrix}$ where: $T^{S1} = T^3$ $T^{S2} = T^3T^2$

takes now the following form (Davis 1988):

$$\begin{Bmatrix} p_o^+ \\ p_o^- \end{Bmatrix} = \begin{bmatrix} S_{11} & S_{12} \\ S_{21} & S_{22} \end{bmatrix} \begin{Bmatrix} p_i^+ \\ p_i^- \end{Bmatrix} + \begin{Bmatrix} p_s^+ \\ p_s^- \end{Bmatrix}, \tag{15}$$

where the source variables are independent of the location of pump ports. According to this representation, the wave travelling in the direction of pump discharge, p_s^+, is directly emitted into the piping system and in our opinion may be used to define the source strength, representing the base pulsation level generated by the pump. The wave travelling in the direction of pump suction, p_s^-, needs to be transferred to the suction port.

As shown by Davis (1988), the relation between the transmission matrix, T, used in equation (14) and the scattering matrix, S, used in equation (15) is

$$\begin{aligned} T_{11} &= \tfrac{1}{2}(S_{11} + S_{12} + S_{21} + S_{22}), \quad T_{12} = \tfrac{1}{2}(S_{11} - S_{12} + S_{21} - S_{22}), \\ T_{21} &= \tfrac{1}{2}(S_{11} + S_{12} - S_{21} - S_{22}), \quad T_{22} = \tfrac{1}{2}(S_{11} - S_{12} - S_{21} + S_{22}), \end{aligned} \tag{16}$$

while the relation between the source variables can be formulated as

$$p_s^+ = \tfrac{1}{2}(p_s + \rho c q_s), \quad p_s^- = \tfrac{1}{2}(p_s - \rho c q_s). \tag{17}$$

Note that, to determine the source characteristics, the source pressure and velocity need to be calculated from equation (17). As discussed already, both may assume a range of values, depending on the location of pump ports. It thus follows that, whichever modelling approach used, the source characteristics may depend on the physical model chosen to represent the pump geometry.

2.2.3. *Transmission characteristics*

As shown in equations (14) and (15), the pump transmission matrix represents a linear relationship between the field variables at the pump discharge and suction ports. Several experimental studies [see, for example, Stirnemann (1987) or Bolleter (1993)] reveal that this relationship can accurately be described with the use of a lumped parameter model of pump elements,

$$T = \begin{bmatrix} 1 + \mathrm{j}\omega C_2 Z_p & Z_p \\ \mathrm{j}\omega(C_1 + C_2 + \mathrm{j}\omega C_1 C_2 Z_p) & 1 + \mathrm{j}\omega C_1 Z_p \end{bmatrix}, \tag{18}$$

where Z_p is the pump acoustic impedance, C_1 and C_2 denote, respectively, the compressibility of the liquid and the elasticity of the walls on the pump suction and discharge sides. These model parameters can be directly linked to the pump and flow characteristics as follows:

$$Z_p = -\rho\left(g\frac{\Delta H}{\Delta Q} - \mathrm{j}\omega\frac{V}{A^2}\right) \tag{19}$$

and

$$C_1 = C_2 = \frac{V_p}{2\rho c^2}. \tag{20}$$

As shown in equation (19), the acoustic impedance contains the real (resistance) and the imaginary (inertance) components. The pump resistance can directly be determined from the head, ΔH, versus flow, ΔQ, curve, while the pump inertance is related to the geometry details of the flow passages within the pump, and can be calculated based on the volume of

water from the suction to the discharge eye of the impeller into the plenum, V, and the average of the suction eye area and the total diffuser throat area, A. Here, the compressibility of the pump suction and discharge sides are assumed to be equal and related to the total pump volume, V_p.

For a stationary pump, the prediction given by equation (18) agrees very well with the measurements of all four elements of the pump transmission matrix (Bolleter 1993). Its application, however, is strongly restricted by the analysis frequency (strictly speaking the acoustic wavelength which has to be significantly larger than the pump dimension, $\lambda \gg D$). For example, for a pump with an impeller of $D = 0{\cdot}35$ m the limit is approximately 100 Hz (Bolleter 1993). A further restriction is cavitation within a pump. Namely, the analysis limit is reached when cavitation starts to manifest itself in a drop of pump head.

2.2.4. *Acoustic sources*

Our main interest in examining the pump acoustic characteristics is to determine the strength of source variables and the acoustic nature of the source (pressure versus velocity). The latter may require a more rigorous treatment of the pump acoustics than that given by equations (14) and (15) which are focused on the simplest physical system while retaining the pump transmission and excitation characteristics.

Due to the flow complexity, it is difficult to classify precisely the flow excitation mechanisms involved in noise generation within centrifugal pumps. The most general classification was recently advanced by Rzentkowski (1996) as (i) the impeller blade and cutwater interaction, (ii) the impeller blade and flow interaction, (iii) the nonuniform outflow from the impeller, and (iv) the vortex structures and flow interaction. These excitation mechanisms can undoubtedly exist simultaneously. Their relative importance may depend on the pump design details and flows, and the acoustic load (impedance) at the pump ports.

Based on the discussion presented by one of the authors (Rzentkowski 1996), we may draw a general conclusion that the acoustic noise at the blade-passing frequency may primarily be generated at the pump exit, due to the nonuniform outflow from the impeller, and at the pump cutwater tip due to the blade/cutwater interaction. The source at the pump exit is equivalent to a velocity source, generating in-phase pressure pulsations at the pump ports, while the source at the pump cutwater is equivalent to a pressure source, generating out-of-phase pressure pulsations. For conventional pump designs, they can approximately be modelled as a single, combined velocity/pressure source positioned at the discharge port. It thus appears that, for most engineering applications, equations (14) and (15) are sufficiently accurate to examine the acoustic characteristics of centrifugal pumps.

Acoustically, when the wavelength is larger than the source, the velocity and pressure sources can be classified as monopole and dipole sources, respectively. The monopole source is characterized by a net mass flow out from the source. In general (free-field wave propagation), the dynamic pressure is proportional to the rate of change of the mass flow (mass flow acceleration) and increases with the square of the flow velocity. The dipole source is characterized by a net force exerted on the flow. The dynamic pressure is proportional to the rate of change of the source force (momentum transfer to the flow) and increases with the third power of the flow velocity.

It has been shown, however, that a piping system can have a profound effect on the radiation properties of the acoustic sources (Nelson & Morfey 1981). For a one-dimensional pressure field considered in this study (plane wave propagation), the acoustic dipole behaves like a free-field monopole; the dynamic pressure increases with the square of the flow velocity. Therefore, a square law between pressure pulsations and circumferential impeller

velocity is used to define the scaling effect between pumps of different size and speed (Guelich & Bolleter 1992).

3. EXPERIMENTAL INVESTIGATION

3.1. Experimental Facility and Procedure

3.1.1. *Test loop*

The pump test loop is shown in Figure 2. The loop consists of the pump legs and headers, and vertical flow elements. The 24 in (0·588 m) diameter pump discharge and suction legs are axially connected to the respective pump headers. The 36 in (0·915 m) diameter headers are linked by three 24 in (0·588 m) diameter vertical flow elements which include flow control valves and Venturi meters. To monitor propagation of pressure waves, several dynamic pressure transducers were installed along the discharge and suction legs, and the inboard vertical flow element. Their exact locations are specified in Table 2. The pressure transducers were flush-mounted in the pipe walls to avoid undesirable amplification, and to ensure accurate measurements. Together with dynamic pressure pulsations, we also monitored the system general conditions such as pump head, loop temperature and pressure, and flow rate.

Prior to the test, the loop was carefully vented and pressurized. The test loop pressure was maintained at 8 MPa on the pump suction by the pressurizing pump (10 MPa on the pump discharge). The loop temperature was gradually increased from the ambient of 20°C to the pump normal operational temperature of 265°C with the use of pump heat. The loop temperature was controlled by an external heat exchanger.

3.1.2. *Test pump*

The test was conducted with a single-stage, mixed-flow, double-volute CANDU heat transport pump that is shown schematically in Figure 3. The fluid flow enters the pump from the suction leg near the impeller centreline, moving parallel to the axis of rotation. Coming between the impeller blades, it is accelerated radially towards the volute. In the volute, the fluid flow moves centrifugally and, passing the volute tongue, is ejected into the discharge leg. Although an individual pump design may differ significantly from that shown in Figure 3, the flow path generally stays the same.

The pump is directly driven by an 8·2 MW (11 000 hp) electric motor. At the normal operational temperature of 265°C, it operates at a rated capacity of 3·3 m^3/s and a head of 213 m. The pump running speed is 1800 r.p.m. (30 Hz). The five-blade impeller is 0·70 m in diameter and 0·159 m in breadth.

3.2. Pressure Measurements

The pressure measurements were recorded with the sampling frequency of 1024 Hz as a function of the process temperature that was recorded with the sampling frequency of 1 Hz. Representative information about pressure amplitudes (zero-to-peak) is provided here by narrow-band spectra averaged over eight data blocks which correspond to eighth-second long acquisition.

Figure 4 illustrates the typical pressure spectrum at the pump operational temperature of 265°C recorded in the pump discharge 2·2 m away from the pump centreline (Location 1 in

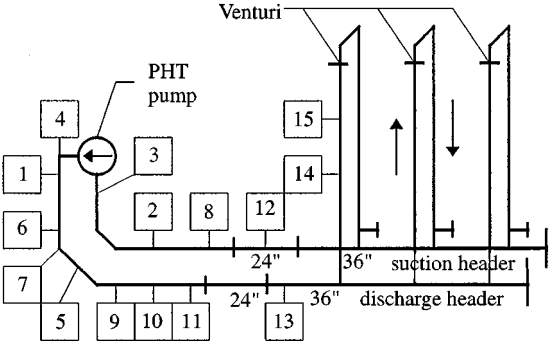

Figure 2. Test-loop layout and instrumentation (numbers indicate location of pressure transducers). The double prime denotes inches (in); 1 in = 25·4 mm.

TABLE 2

Pressure measurement locations in the pump discharge and suction (distance measured from pump centreline)

Pump discharge side		Pump suction side	
Location	Distance (m)	Location	Distance (m)
4	0·864	12	7·314
1	2·278	8	5·514
6	2·978	2	4·815
7	4·641	3	2·260
5	5·201		
9	6·224		
10	6·924		
11	7·624		
13	12·179		
14	20·332		

Figure 2). We believe that at this location the effect of hydraulic noise (convective terms) is significantly reduced and the pressure spectrum contains predominantly acoustic noise. It consists of turbulence, which manifests itself as a broad-band process in a low-frequency range (below 40 Hz), and the discrete excitations at 30 Hz, associated with the pump running speed, and at 150 Hz caused by the periodic passage of impeller blades (5×30 Hz). The peaks at 60 and 300 Hz represent, respectively, the second harmonic of the pump running speed and the blade-passing frequency. Clearly, the blade-passing excitation at 150 Hz represents the potentially harmful component of the pressure spectrum.

Figure 5 shows the dynamic pressure pulsations at the blade-passing frequency measured at the pump discharge and suction (Locations 6 and 2, respectively). This figure reveals that the pump-generated pressure pulsations show a strong effect of the loop acoustics associated with an increase in the loop temperature. The peak amplitude varies by almost a factor of 10 in the tested temperature range, revealing a clear resonance in the test loop at 256°C. At the resonance, the peak amplitude reaches 23 kPa in the pump discharge and 8 kPa in the pump suction. It should be realized that the effect of temperature on the test loop acoustics, documented in Figure 5, is approximately equivalent to a source frequency sweep. As we show later, the speed of sound decreases from 1423 to 1059 m/s in the

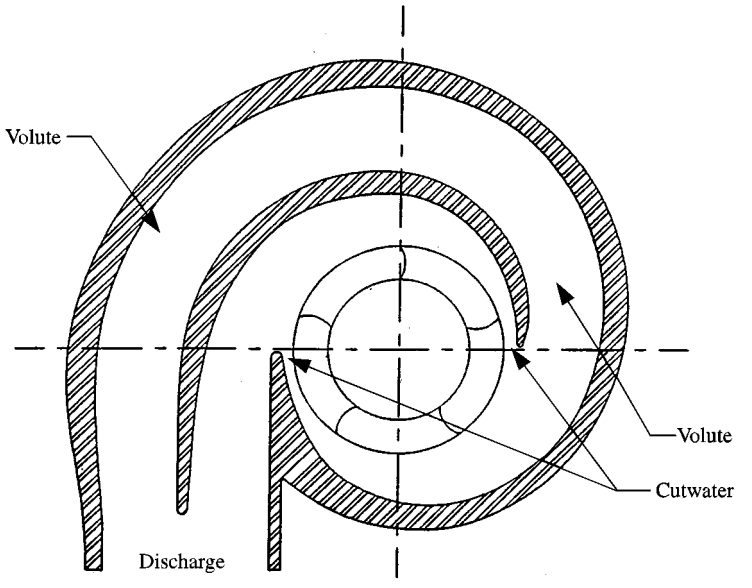

Figure 3. Schematic representation of a double-volute CANDU Heat Transport pump.

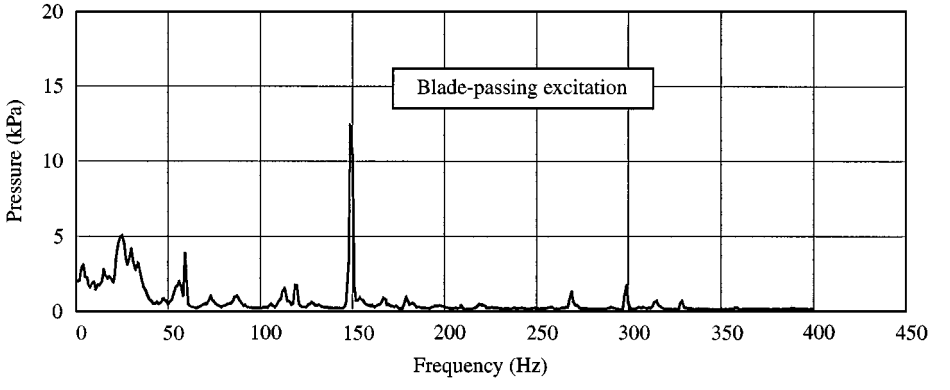

Figure 4. Typical pressure spectrum in the pump discharge leg at 265°C.

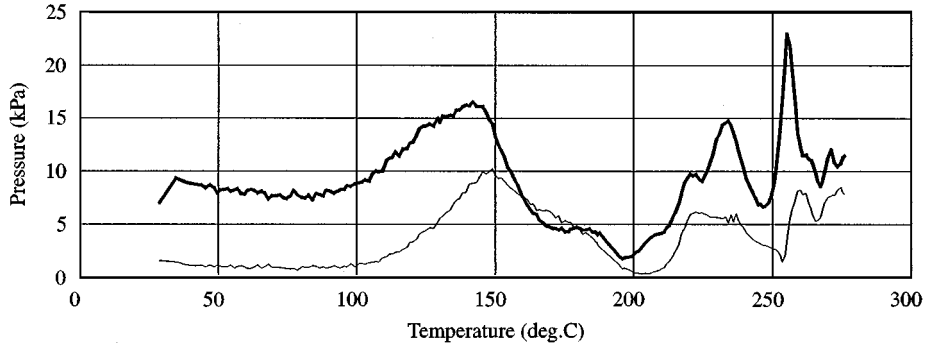

Figure 5. Blade-passing pressure pulsations in the pump discharge and suction legs as a function of test-loop temperature. Thick line: discharge; thin line: suction.

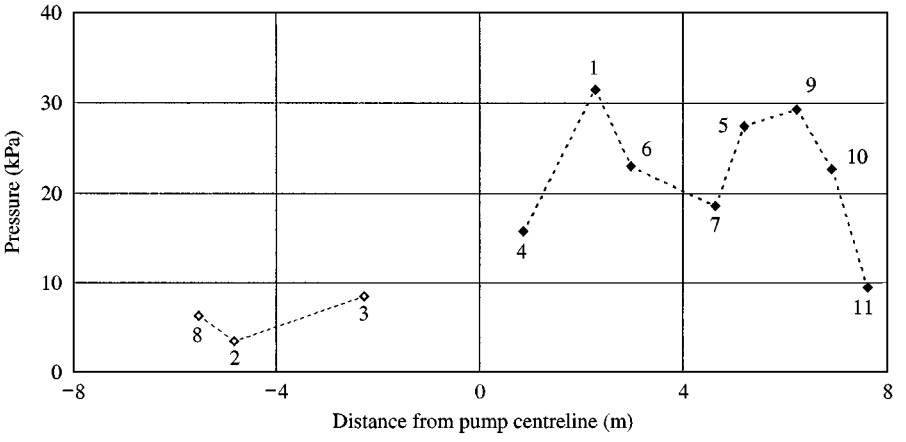

Figure 6. Blade-passing pressure pulsations in the pump discharge and suction legs at the loop-resonance (256°C): -◇-, pump suction; -◆-, pump discharge.

temperature range from 20 to 270°C. As a result, the acoustic wavelength decreases from 9·49 to 7·06 m. The corresponding change in the acoustic wavelength would be observed if the excitation frequency was swept from 112 to 150 Hz at the constant temperature of 265°C.

To better illustrate the aforementioned acoustic resonance in the test loop, Figure 6 shows the dynamic pressure measurements recorded along the discharge and suction legs at 256°C (numbers near data points indicate measurement locations, while the dashed line is used to emphasize variations in dynamic pressure along the pump discharge and suction legs). As depicted in this figure, a strong effect of loop acoustics on the pump-generated pressure pulsations can be identified especially in the pump discharge. The peak pressure amplitude varies by approximately a factor of three with the distance away from the pump, approaching 32 kPa at Location 1 near the pump discharge port. In the pump suction, the peak pressure amplitude does not exceed 10 kPa.

4. ANALYSIS OF PRESSURE MEASUREMENTS

4.1. Test Loop Acoustics

Figures 5 and 6 reveal that the pressure measurements at the pump suction and discharge may significantly vary with the loop temperature and with the distance away from the pump, due to the resonance effects in the test loop. To examine these effects, we first decompose the local pressure field into travelling wave components. We also assess the qualitative effect of any disturbance in the local pressure field, which may interfere with the pressure measurements. Next, we conduct the mode-shape analysis to confirm the one-dimensionality of the pressure field, and to calculate the acoustic impedance and the reflection coefficient at the pump ports.

Figure 7 shows the results of pressure field decomposition in the pump discharge and suction legs (Locations 6 and 2), respectively; i.e., the results of numerical solution of equations (6) and (7). In general, the travelling waves show less variation with the loop temperature than the total acoustic pressure (see Figure 5 for comparison). The trends, however, are similar showing the distinct resonant peaks at 256°C. At the loop resonance, the sum of peak amplitudes of the waves travelling in opposite directions is approximately

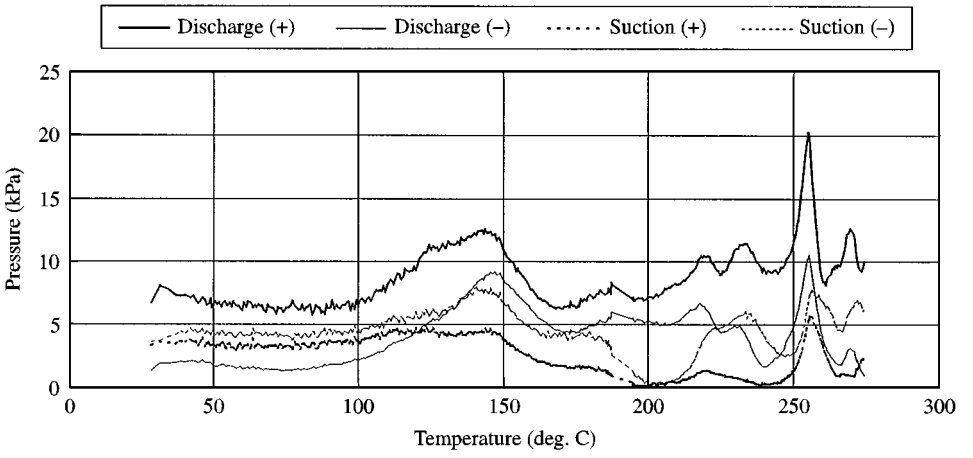

Figure 7. Decomposition of acoustic pressure field into travelling components in the pump discharge and suction legs: (+) positive and (−) negative directions.

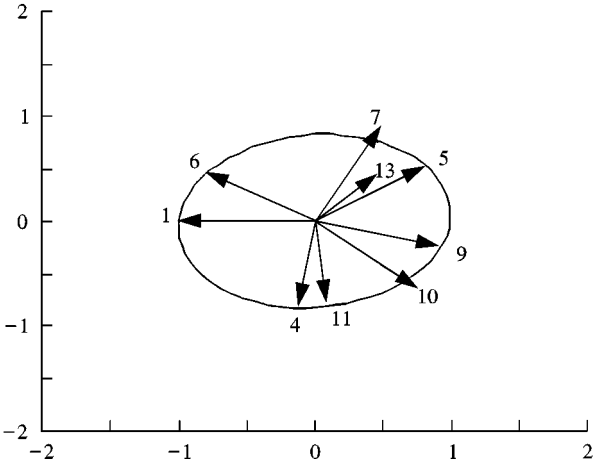

Figure 8. An ellipse formed by acoustic pressure in the pump discharge leg.

equal to the total acoustic pressure at the pump discharge and suction, respectively, meaning that the corresponding travelling waves are in phase.

It should be appreciated that the pressure field decomposition is very sensitive to measurement errors and, if equations (3) and (4) are used, the transducer spacing. Therefore, the qualitative assessment of pressure measurements is necessary in order to warrant the analysis of the pressure field. As an example, Figure 8 shows an ellipse derived from pressure measurements at the pump discharge. These measurements (numbers indicate measurement locations), both magnitude and phase, are normalized against pulsations at Location 1. It can be seen that, for all the transducers positioned on the 24-in discharge pipe, the assumed ellipse fits well onto the experimental points. (In contrast, the pressure measurements in the 36-in header pipe, Location 13, diverge significantly due to reflective characteristics of a reducer.) This indicates that the measured pressure satisfies the one-dimensional pressure field in the pump discharge leg. Small qualitative differences between the predicted and measured pressure can conceivably be attributed to random measurement errors.

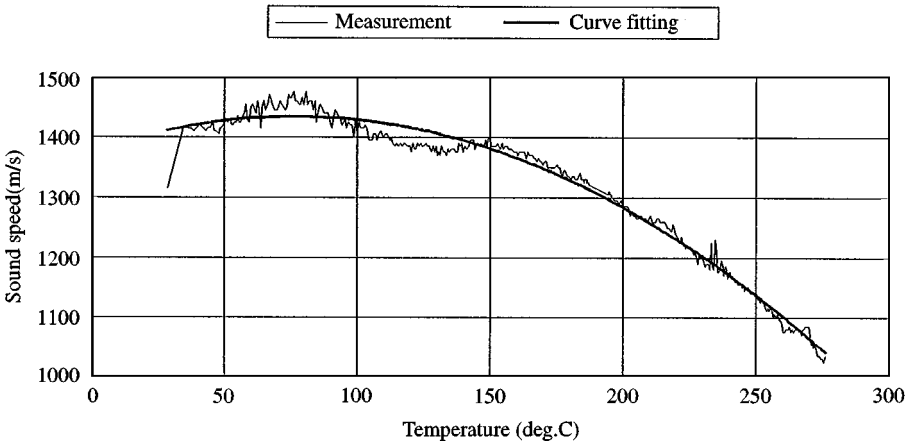

Figure 9. Speed of sound estimation in the test loop.

The pressure field decomposition requires also the speed of sound in a piping system at each temperature level. For this, we use the system identification procedure formulated to solve equations (6) and (7). The results of this investigation, together with a least-square error smoothing curve, are shown in Figure 9. It can be seen that, as expected, the speed of sound increases initially with temperature, reaching a maximum of approximately 1450 m/s at 80°C, and then decreases gradually to approximately 1050 m/s at 275°C. The least-square curve-fitting technique yields the following relationship between the speed of sound and the system temperature (Rzentkowski & Zbroja 1997):

$$c = 1368 + 1{\cdot}61t - 0{\cdot}0102t^2, \tag{21}$$

where c is the speed of sound expressed in m/s and t is the system temperature in °C. We use equation (21) in the subsequent analysis to calculate the speed of sound as a function of loop temperature.

With the acoustic pressure field fully decomposed, we can use equation (5) to conduct the mode-shape analysis in the pump discharge and suction legs. We consider both the pressure amplitudes and phases. Figure 10 shows an example of this analysis for quasi-anechoic (240°C) and highly reflective conditions in the test loop (256°C). The predicted mode shapes are represented by solid lines, and the measured pressure by markers. For completeness, the results of pressure field decomposition are also included in Figure 10; the left and right pointing arrows represent amplitudes of travelling waves. These results lead to two important observations. First, the pump introduces a jump in a local pressure field that confirms the superposition principle assumed in this study to represent the source variables [see equations (14) and (15)]. Second, there is a very good agreement, in both amplitude and phase, between the predicted mode shapes and pressure measurements. The latter confirms the one-dimensionality of the pressure field.

Figures 11 and 12 show, respectively, the magnitude of the acoustic impedance and the reflection coefficient at the pump discharge (Location 6) and suction (Location 2) calculated from equations (11) and (12), together with equation (10). Both show a strong effect of temperature. The magnitude of the acoustic impedance oscillates around the value of one which is characteristic for an infinite pipe (nonreflective termination). The magnitude of the reflection coefficient varies between zero and one, approaching a minimum at the pump suction and discharge at the same temperature of approximately 240°C. At this temperature, the analysed system can be treated as quasi-anechoic; the effect of loop resonance is

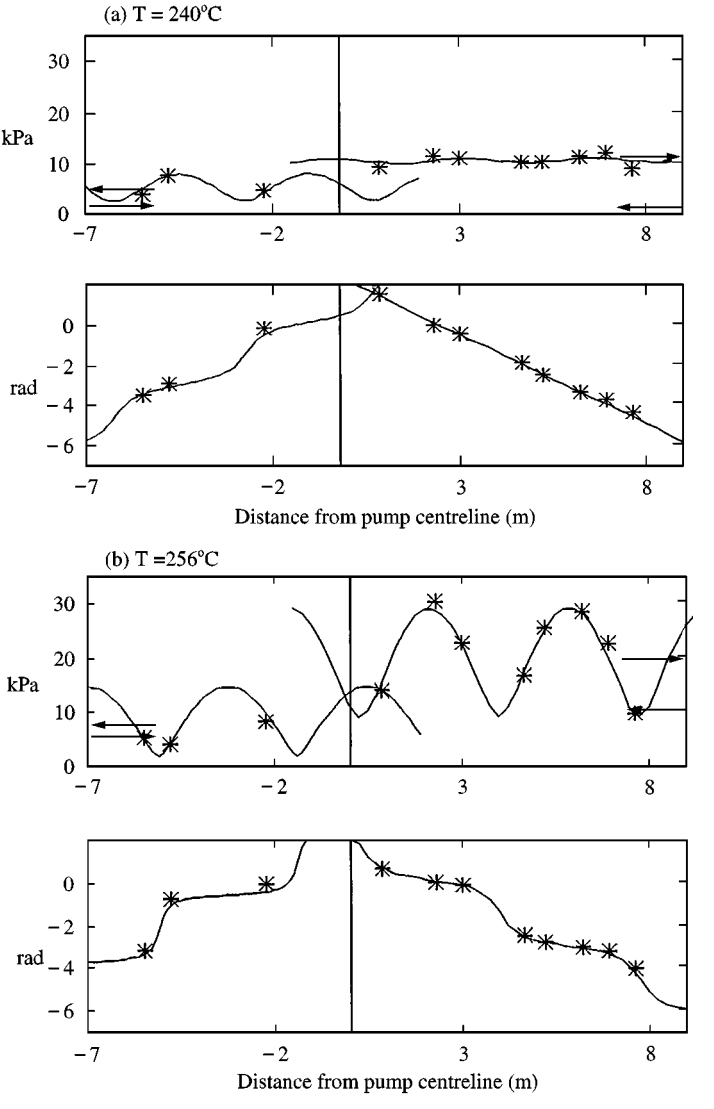

Figure 10. Acoustic mode-shape analysis (pressure amplitude and phase) of the pressure field in the pump discharge and suction legs: (a) nonreflective and (b) reflective termination.

significantly limited, since the local pressure field is dominated by the waves travelling away from the pump (acoustic impedance equal to one).

4.2. Pump Acoustics

For the purpose of this analysis, we consider both the one- and two-port pump representations. We assume that the pump ports are positioned at a straight section of pipe directly upstream and downstream of the pump, as shown schematically in Figure 13. Keeping with the pump geometry (see Figure 3), this implies that the two-port pump model includes the flow passages within the pump volute. As follows from equations (18) and (19), their

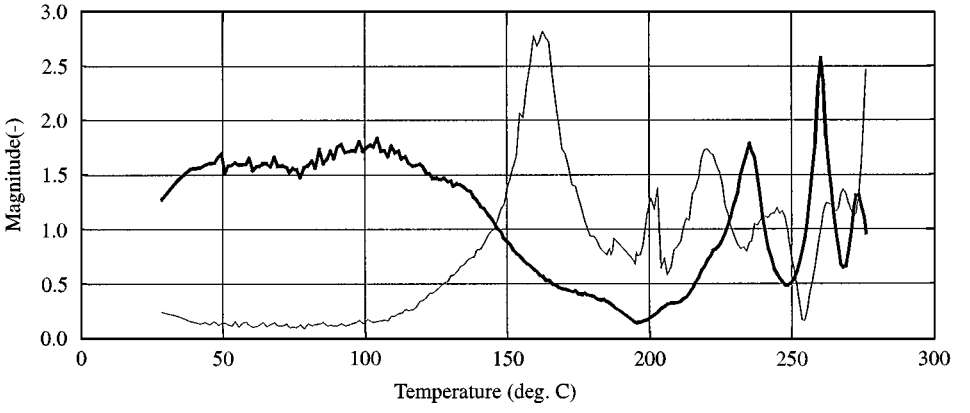

Figure 11. Magnitude of acoustic impedance at the pump discharge and suction. Thick line: discharge; thin line: suction.

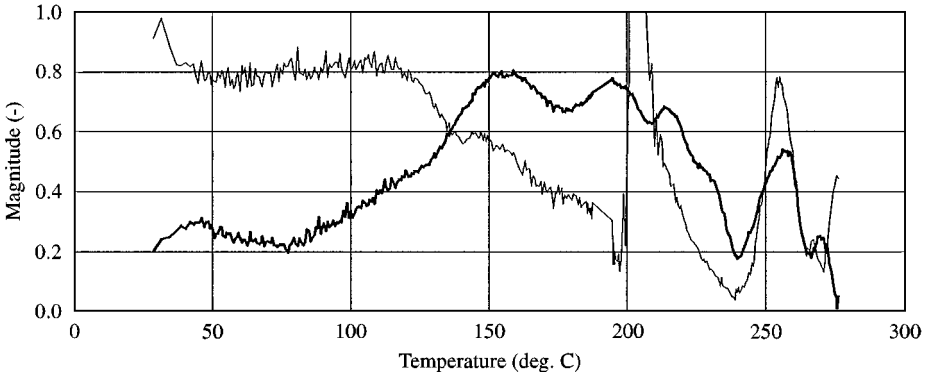

Figure 12. Magnitude of reflection coefficient at the pump discharge and suction. Thick line: discharge; thin line: suction.

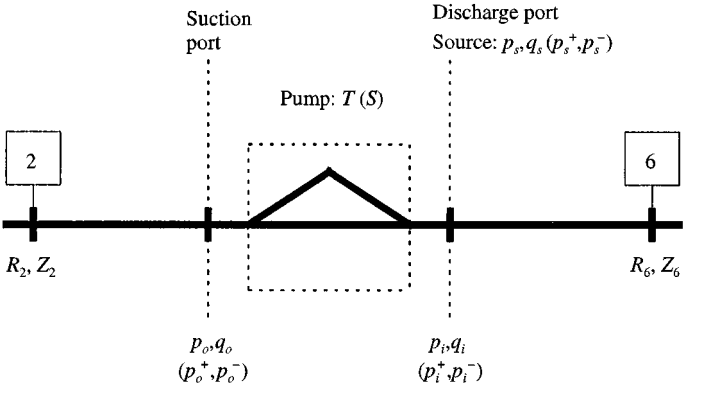

Figure 13. An equivalent one-dimensional model of the pump and the adjacent piping system based on the transmission (T) and scattering (S) matrix representations.

effective acoustic transmission is predominantly governed by the pump impedance, Z_p [$C_1 = C_2 \approx 0$ in equation (20)]. We may thus reduce equation (18) to the following form:

$$T = \begin{bmatrix} 1 & Z_p \\ 0 & 1 \end{bmatrix}. \tag{22}$$

Figure 14 shows the real (resistance) and imaginary (inertance) parts of the pump impedance calculated from equation (19). Both are normalized by ρc. Evidently, due to the lack of direct measurements for the pump examined here, uncertainty exists in the quantitative results. We thus examine the sensitivity of the model's predictions to the pump impedance by independently varying the real and imaginary parts by $\pm 100\%$ from the baseline values shown in Figure 14. This simplified uncertainty analysis reveals that the model's predictions are not critically dependent on the pump impedance. We thus use the baseline value of Figure 14 in the subsequent analysis of the pump acoustics.

4.2.1. *Source variables*

We attempt here to determine the source variables with the objective to isolate an acoustic source from the pressure measurements in the test loop and to compare the predictions of the transmission and scattering matrix pump models. First, however, we assess the qualitative effect of coupling between the field variables at the pump ports by comparing the source pressure as related to the single-port pump model, equation (12), and as related to the two-port pump model, equation (14). Figure 15 shows the respective numerical results, together with the pressure measured at the pump discharge (Location 6 in Figure 2). By comparing these results, we show clearly that the models' predictions may differ quite drastically. The single-port model, a "blocked" pressure source, is strongly dependent of the system acoustics. The source pressure is approximately equal to the pump port pressure, $p_s \cong p_o$, which varies by an order of magnitude, and cannot be used for quantitative estimation of the source strength. The two-port pump model, on the other hand, is less sensitive to the loop acoustics; the source pressure is relatively constant in comparison with the measured port pressure. Interestingly, the difference between the two models is less pronounced at higher temperatures due to, conceivably, shortening of acoustic waves and thus increasing reflection at the pump. This observation leads to the conclusion that the coupling effects between the field variables at the pump ports decreases with the excitation frequency.

Figure 16 shows the source pressure and velocity for the two-port pump representation which are calculated from equation (14). The source velocity is expressed as $\rho c q_s$, for direct comparison. As depicted in Figure 16, the effect of loop acoustics on the source pressure and velocity does not manifest itself as clearly as on the pressure measurements documented in Figure 5, although both show an increasing trend with the loop temperature. The source pressure can be estimated at 12 ± 5 kPa, while the source velocity is 12 ± 8 kPa. The source variables associated exclusively with pump action can be estimated from measurements conducted at 240°C (the magnitude of reflection coefficient approaches zero in the pump discharge and suction, as shown in Figure 12). These measurements yield approximately 10 kPa for both the source pressure and velocity. Note that the source pressure corresponds closely to the pump discharge pressure at 240°C (see Figure 5).

Figure 17 shows the amplitude of the pressure waves emitted by the pump in the positive (pump discharge) and negative (pump suction) directions for the two-port pump representation which are calculated from equation (15). It can be seen that both pressure waves behave similarly as the corresponding source pressure and velocity, showing also an increasing

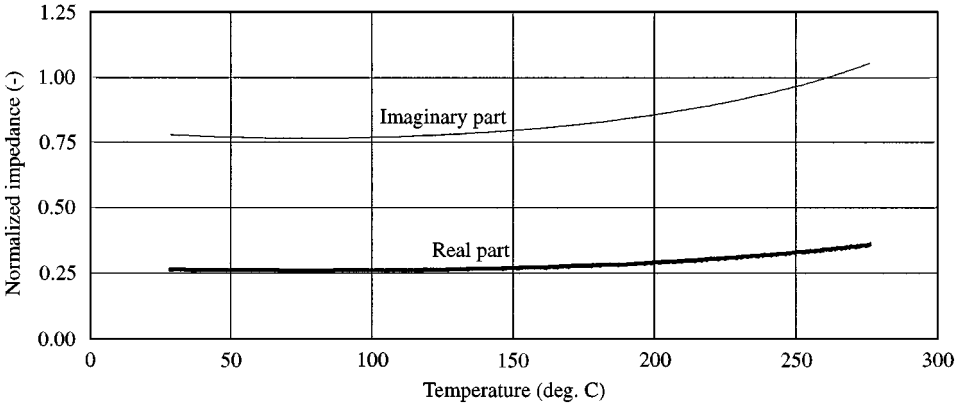

Figure 14. Normalized real (resistance) and imaginary (inertance) parts of the pump acoustic impedance utilized to formulate the pump transmission matrix.

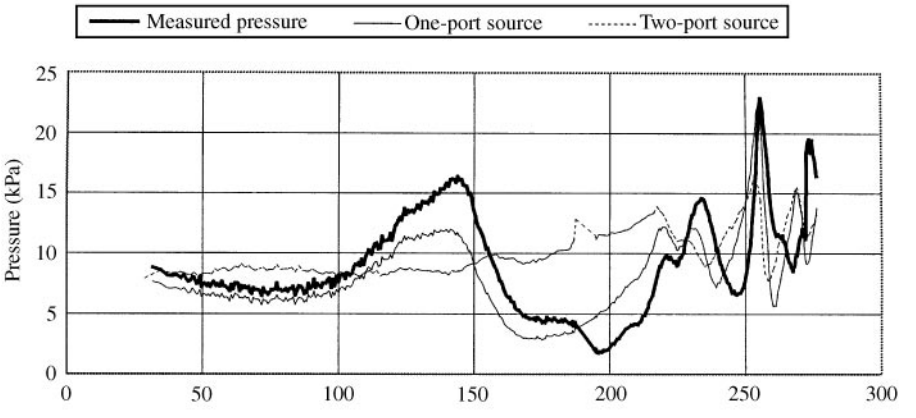

Figure 15. Estimation of the pump source pressure with the pump modelled as a one-port and as a two-port system.

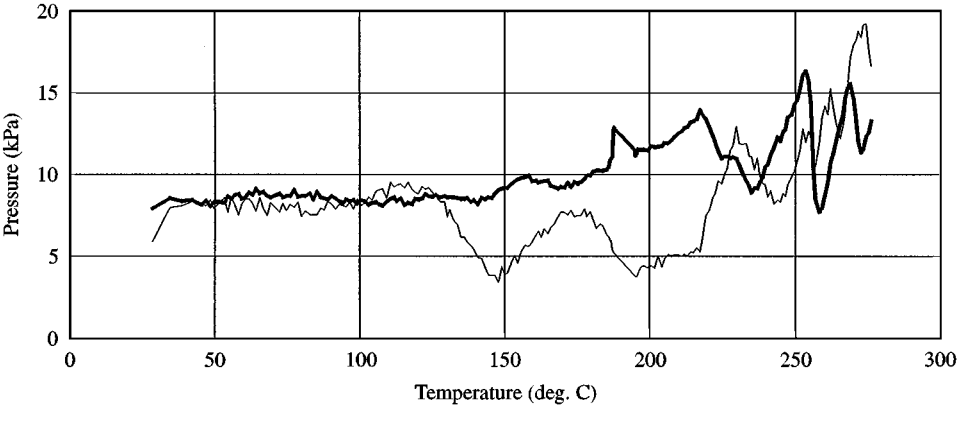

Figure 16. Estimation of pump acoustic variables at the pump discharge port using the transmission matrix approach (source pressure and velocity). Thick line: source pressure; thin line: source velocity.

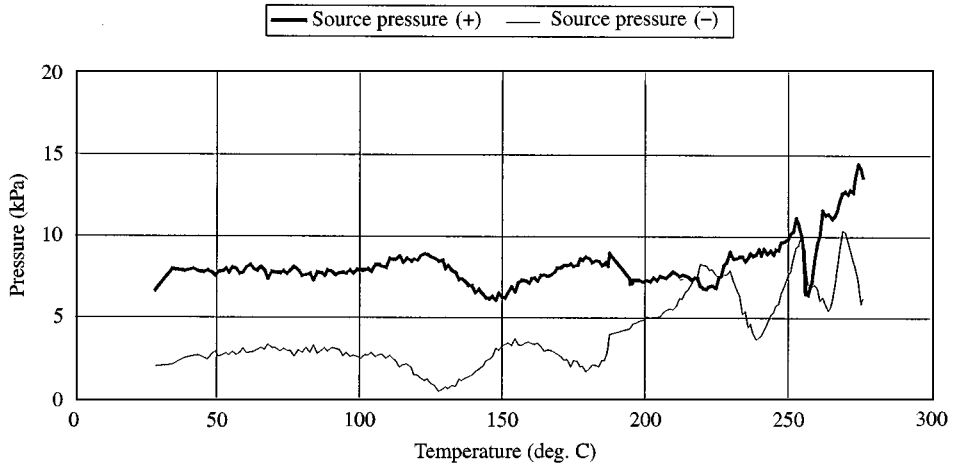

Figure 17. Estimation of pump acoustic variables at the pump discharge port using the scattering matrix approach (source pressure waves travelling in opposite directions).

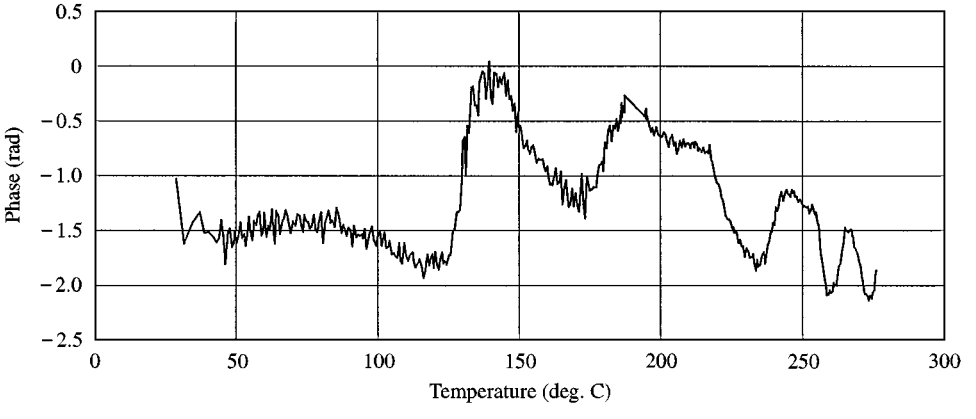

Figure 18. Phase relationship between pressure waves emitted by the source in the directions of pump discharge and suction.

trend with the loop temperature. The source variables can be estimated at 10 ± 4 kPa for the pressure wave travelling in the direction of pump discharge and 5 ± 5 kPa for the pressure wave travelling in the direction of pump suction. The peak amplitudes associated exclusively with the pump action are, respectively, 9 and 5 kPa (measurements at 240°C). This is in a very good agreement with the results of equation (14) and with the direct measurements of the pump discharge and suction pressures. It is worth to recall that, in a straight section of piping, the results of equation (15), as opposed to equation (14), are independent of the measurement location. Thus, the amplitude of the pressure waves emitted in the direction of the pump discharge may be used to define the source strength; the base pulsation level generated by the pump. Note that, on average, this amplitude is lower than the source pressure calculated from equation (14). This may conceivably be attributed to the effect of acoustic amplification, manifesting itself at the pump port.

Figure 18 shows the phase relationship between the pressure waves emitted by the source in the directions of pump discharge and suction. It reveals a strong effect of loop

temperature. Initially, the pressure waves are generated with a constant phase of about 90°. This suggests that the pump simultaneously introduces a mass flow and a force, and thus acts as a combined velocity and pressure source. At 140°C, the phase undergoes a step change to zero degrees. The pressure waves are generated in phase, introducing a net mass flow out from the source. This suggests the pump acts as a velocity source. Next, the pressure waves generated move gradually out of phase as the loop temperature is increased. In general, the pump acts as a combined source. At the loop resonance of 256°C, the pressure waves are approximately out of phase, introducing a net force. The pump thus acts as a pressure source. There are, however, random deviations from this trend. Therefore, we shall examine the source acoustic characteristics by a means of separate analysis in the following section.

4.2.2. *Source characteristics*

To determine the acoustic nature of the pump, we assess the relative importance of the source variables in exiting the local pressure field in the pump vicinity. For this, we calculate the system pressure at the pump suction and discharge with the pump acting either as a pressure source, $q_s = 0$ in equation (14), or as a velocity source, $p_s = 0$ in equation (14). As before, the system boundary impedance at the pump discharge and suction ports are estimated experimentally. Figures 19 and 20 compare the model's predictions with the pressure measured at the pump discharge and suction (Locations 6 and 2 in Figure 2, respectively). In both cases, the sum of acoustic pressure generated separately by the velocity and pressure sources is equal to the measured pressure. It can be seen that, for the pump model examined here, the pump may act either as a velocity or as a pressure source. The velocity term predominates at low temperatures. The pressure term, on the other hand, almost exclusively dominates the acoustic field in the pump vicinity at high temperatures, including the loop resonance. This effect is especially pronounced at the pump discharge (see Figure 19), and agrees with the results of Figure 18.

5. DISCUSSION OF PUMP ACOUSTICS

We can examine the pump acoustics only to the extent the underlying pump model captures the physics of noise generation and includes the key details of the pump geometry essential for transmission characteristics. Based on experimental evidence, we limit here the pump modelling to the linear superposition of acoustic wave transmission and excitation. We assume further that acoustic waves are excited by a single-point source positioned at the pump discharge port (see Figure 13). We do not attempt to explore the underlying flow excitation mechanisms. We show, however, that the acoustic field in the pump vicinity has both monopole and dipole characteristics. This leads us to believe that the blade/tongue interaction (dipole source) may represent the primary mechanism involved in generation of acoustic noise at the blade-passing frequency, while the nonuniform outflow from the impeller (monopole source) represents the secondary mechanism. It must be realized that this conclusion may not be true in general since the strength of acoustic sources within centrifugal pumps depends on the pump size and speed, and the design details of pump geometry (Rzentkowski 1996). Nevertheless, based on the hypothesis advanced above, we may redefine the "black box" approach utilized in this study to formulate the pump model. As shown in Figure 21, we assume that the double-volute pump may have two pressure sources, each positioned near the cutwater tip, and a single velocity source at the pump exit. It must be appreciated that the length of acoustic paths within the pump cannot be assessed exactly due to the three-dimensionality of the pump volute. They are defined here based

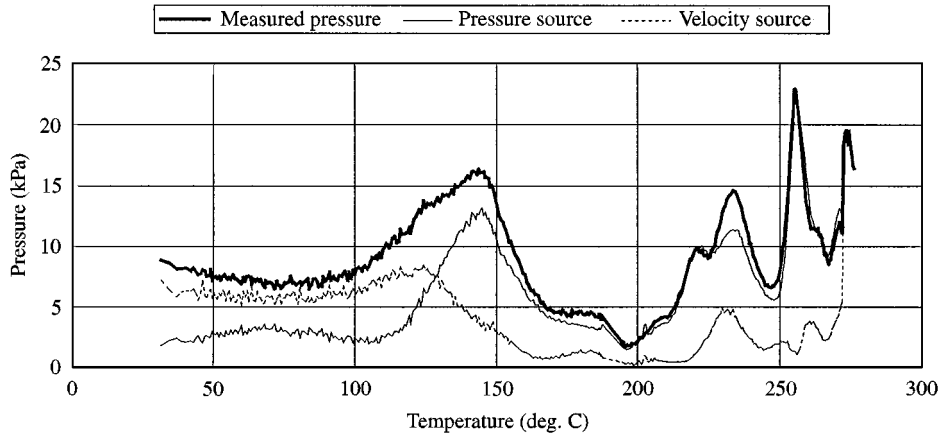

Figure 19. Estimation of pressure pulsations at the pump discharge with the pump modelled as a combined pressure and velocity source at the pump discharge port.

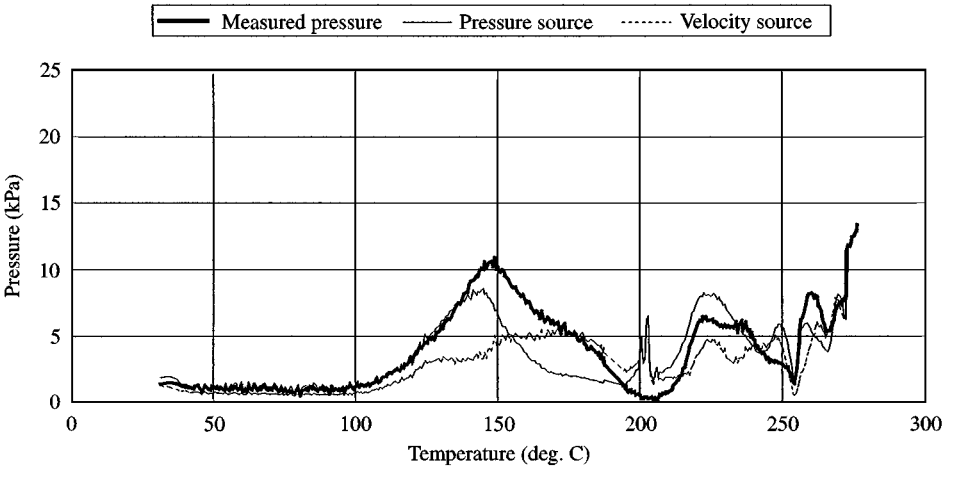

Figure 20. Estimation of pressure pulsations at the pump suction with the pump modelled as a combined pressure and velocity source at the pump discharge port.

directly on one-dimensional geometrical considerations and thus they may be somewhat idealized.

Since the pump volute is symmetrical, we may also assume that the pressure sources are of equal strength and act out of phase independently of each other. Thus, the pressure and velocity variables at the pump discharge port represent linear superposition of acoustic waves generated at each source. Figure 22 shows the results of simultaneous action of both pressure sources normalized against the source pressure at the cutwater tip. Clearly, the effect of superposition tends to increase the strength of source pressure at the pump discharge and decrease the strength of source velocity with increasing temperature. It is important to note that the velocity term at the pump discharge is exclusively associated with the pressure term introduced at the cutwater tip. Thus, only the residual velocity term, the difference between the source velocity of a combined source at the pump discharge port

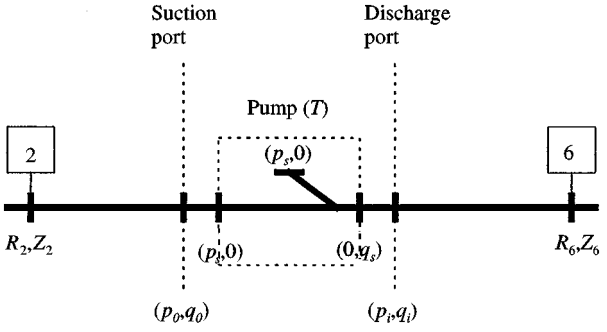

Figure 21. An equivalent one-dimensional, multi-source model of the pump and the adjacent piping system based on the transmission (T) matrix representation.

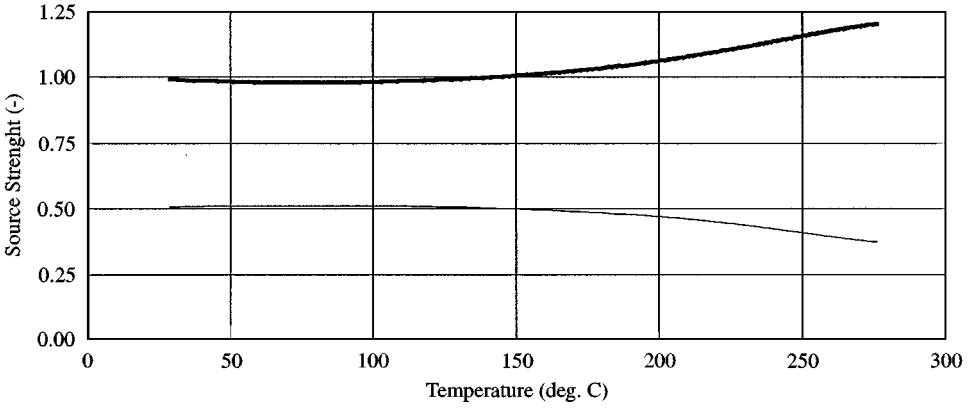

Figure 22. Estimation of pump acoustic variables at the pump discharge port with the pump modelled as a pressure source at the cutwater (results are normalized against the pressure magnitude at the cutwater). Thick line: source pressure; thin line: source velocity.

(see Figure 16) and the source velocity related to the pressure source at the cutwater, can be attributed to the presence of the velocity source at the pump exit.

Figure 23 shows the strength of the acoustic sources illustrated schematically in Figure 21; i.e., the source pressure at the cutwater tip and the source velocity at the pump exit. The source pressure can be estimated at 10 ± 4 kPa, while the source velocity is 4 ± 2 kPa. As follows from equation (19), the magnitude of incident waves generated at the cutwater tip is half of the source pressure, while the magnitude of incident waves generated at the pump exit is half of the source velocity. The first can thus be estimated at 5 ± 2 kPa and the latter at 2 ± 1 kPa (note that the wave travelling in the direction of pump discharge has a positive sign whereas the wave travelling in the direction of pump suction has a negative sign). Figure 23 reveals that the mean value of the source pressure and velocity is almost constant in the tested temperature; the increasing trend documented in Figures 16 and 17 is no more visible. It thus appears that an increase in the source strength in Figures 16 and 17 may conceivably be attributed to the interaction of the pressure waves generated at the cutwaters and not to the resonance effects in the test loop. Further, we may also conclude that the source strength is exclusively related to pump action. Evidently, some variations in the predicted source strength are unavoidable because the solution of equations (14) and (15) is susceptible to random measurement errors.

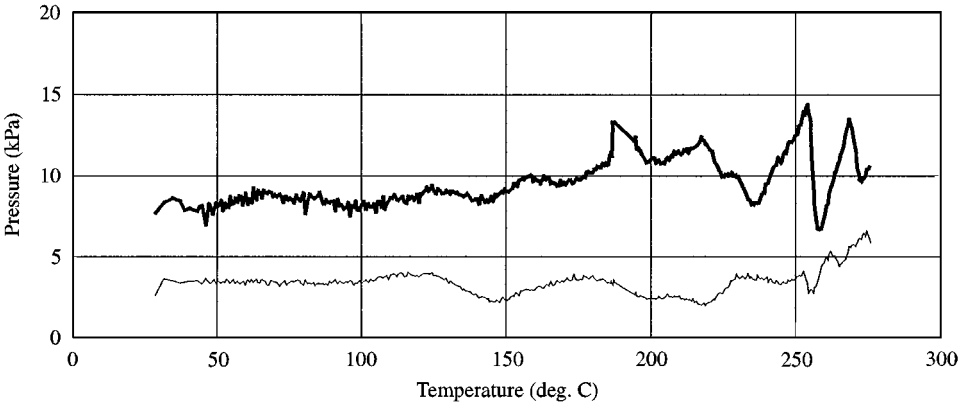

Figure 23. Estimation of pump acoustic variables at the pump discharge port with the pump modelled as a pressure source at the cutwater. Thick line: source pressure; thin line: source

We also examine the acoustic nature of the pump with the use of the redefined pump model. The numerical procedure is analogous to that applied to generate Figures 20 and 21. First, we calculate the system pressure at the pump suction and discharge with the pump acting either as the pressure source at the cutwater tip or as the velocity source at the pump exit. Next, we compare the predictions with the pressure measured at the pump discharge and suction (Locations 6 and 2 in Figure 2, respectively). The results of this analysis are presented in Figures 24 and 25. Only subtle quantitative differences can be identified in comparison with Figures 19 and 20. Qualitatively, the results are identical. This confirms the conclusion drawn previously that the pump may act either as a velocity or as a pressure source. Conceivably, the relative importance of acoustic sources may depend on the pump transmission characteristics and/or acoustic load at the pump ports.

6. CONCLUSIONS

This study describes an experimental method to examine the pump acoustic characteristics at the blade-passing frequency. The method is based on an analysis of the pressure field in the pump suction and discharge, and a simple pump model based on a linear superposition of pressure wave transmission and excitation. It allows one to isolate the pump-generated pressure pulsations from the pressure measurements local to the pump.

We applied this method to a single-stage, double-volute pump. The analysis leads to some general conclusions regarding the pump acoustic modelling and test data analysis. They can be summarized as follows.

(i) The pump should be modelled with the use of a general two-port representation allowing for transmission of acoustic waves between the pump ports.

(ii) The two-port pump model can be formulated as a linear superposition of pressure wave transmission (transfer matrix) and excitation (source variable). The model's predictions are not critically dependent on the parameters related to pump geometry.

(iii) The source variables represent a jump in the acoustic field: either pressure or/and velocity (transmission matrix), or waves travelling in opposite directions (scattering matrix). They appear to be free of the effects of acoustic resonance in the test loop.

(iv) The scattering matrix approach is independent of the pump port location within a piping system and thus gives a more convenient description of pump acoustics. The

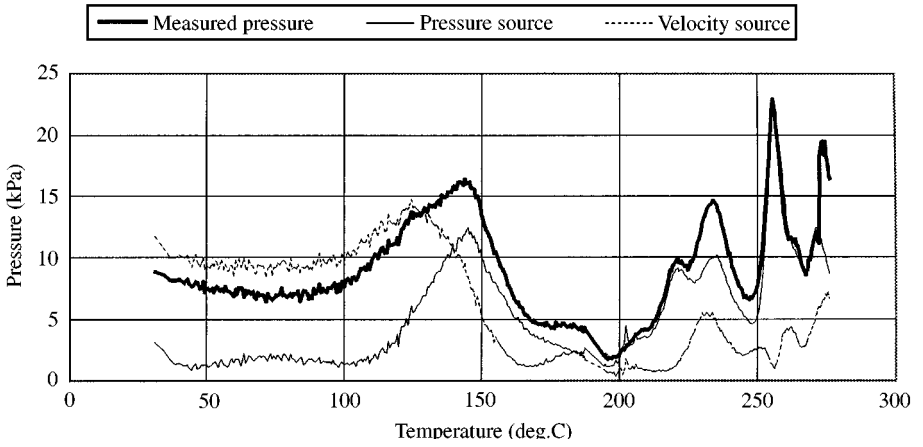

Figure 24. Estimation of pressure pulsations at the pump discharge with the pump modelled as a pressure source at the cutwater and as a velocity source at the pump exit.

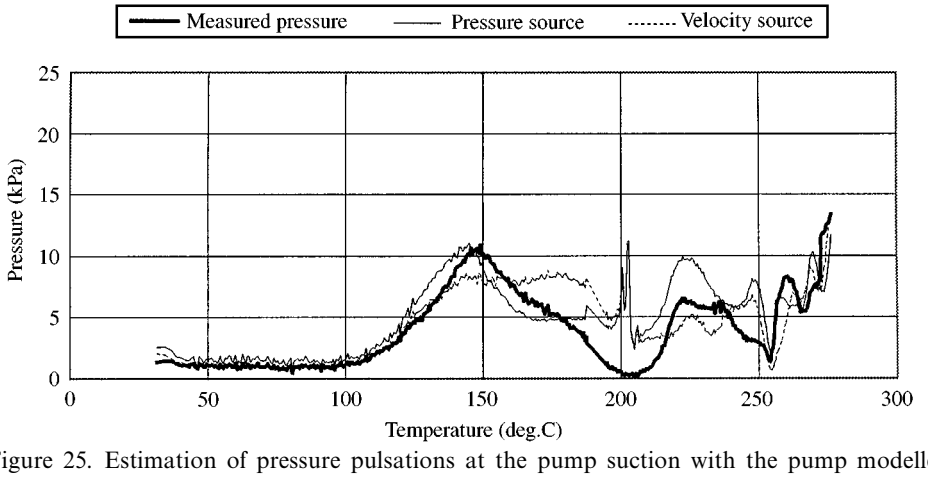

Figure 25. Estimation of pressure pulsations at the pump suction with the pump modelled as a pressure source at the cutwater and as a velocity source at the pump exit.

pressure wave travelling in the direction of pump discharge should be used to define the pump pulsation level for valid comparison between different designs and for acoustic modelling of piping systems.

(v) The pump may act either as a pressure or as a velocity source, depending on the transmission characteristics and/or test loop acoustics.

We feel that the approach presented in this study is a promising tool to serve as a universal technique for examining the pump acoustic characteristics and for reporting the test data. Definitely, it is simple enough for engineering applications.

ACKNOWLEDGEMENTS

The authors thank the staff of the Nuclear Plant Component Testing Facility of Ontario Hydro Technologies for instrumenting and operating the pump test loop. Especially, the

authors express their sincere appreciation to Mr S. Barreca for his help in test preparation and execution. Also, the authors thank the management of Ontario Hydro Technologies for permission to publish the test-data.

References

Bolleter, U. 1993 Interaction of pumps and piping systems with regard to pressure pulsations. *Proceedings 1st International Symposium on Pump Noise and Vibrations*, Clamart, France, pp. 3–10.

Chaudhry, M. H. 1986 *Applied Hydraulic Transients*. Princeton, NJ: Van Nostrand Reinhold.

Chu, S., Dong, R. & Katz, J. 1993 The effect of blade-tongue interaction on the flow structure, pressure fluctuations and noise within a centrifugal pump. *Proceedings 1st International Symposium on Pump Noise and Vibrations*, Clamart, France, pp. 13–24.

Chung, J. Y. & Blaser, D. A. 1980a Transfer function method of measuring in-duct acoustic properties. I. Theory. *Journal of the Acoustical Society of America* **68,** 907–913.

Chung, J. Y. & Blaser, D. A. 1980b Transfer function method of measuring in-duct acoustic properties. II. Experiment. *Journal of the Acoustical Society of America* **68,** 914–921.

Davis, P. 1988 Practical flow duct acoustics. *Journal of Sound and Vibration* **124,** xxx–yyy.

De Jong, C. A. F. 1994 Analysis of pulsations and vibrations in fluid-filled pipe systems, Ph.D. Thesis, Eindhoven University of Technology, Endhoven, The Netherlands.

De Jong, C. A. F., Krieseles, P. C., Bruggeman, J. C. & Van Bokhorst, E. 1993 Measurement of the characteristics of a centrifugal pump as a source of pressure pulsations. *Proceedings 1st International Symposium on Pump Noise and Vibrations*, Clamart, France, pp. 167–174.

Edge, K. A. & Johnston, D. N. 1990 The "Secondary Source" method for the measurement of pump pressure ripple characteristics. Part 1: description of the method. *Proceedings Institution of Mechanical Engineers* **204,** xx–yy.

Guelich, J. F. & Bolleter, U. 1992 Pressure pulsations in centrifugal pumps. *ASME Journal of Vibration and Acoustics* **114,** 272–279.

Morse, P. M. & Ingard, K. U. 1986 *Theoretical Acoustics*, New York: McGraw-Hill.

Nelson, P. A. & Morfey, C. L. 1981 Aeorodynamic sound production in low speed flow ducts. *Journal of Sound and Vibration* **79,** 263–289.

Rzentkowski, G. 1996 Generation and control of pressure pulsations emitted from centrifugal pumps: a review, *ASME PVP Conference* Montreal, Canada; PVP-vol. 328, pp. 439–454.

Rzentkowski, G., Forest, J. W. & Martin, D. G. 1993 Acoustical characterization of the heat transport system of Darlington nuclear generation station: analysis technique and results. *Proceedings 1st International Symposium on Pump Noise and Vibrations*, Clamart, France, pp. 289–300.

Rzentkowski, G. & Zbroja, S. 1997 Acoustic characterization of a CANDU primary heat transport pump. *Proceedings 5th International Conference of Nuclear Engineering, ICONE-5*, Nice, France

Simpson, H. C., Clark, T. A. & Weir, G. A. 1967 A theoretical investigation of hydraulic noise in pumps. *Journal of Sound and Vibration* **5,** 456–488.

Stirnemann, A. 1987 Using the transfer matrix notation to describe the stability of hydraulic systems. *Proceedings IAHR Work Group on the Behavior of Hydraulic Machinery under Steady Oscillating Conditions*, Lille, France.

Whitson, R. J. & Benson, I. M. 1993 Investigation of the fluidborne noise source and source impedance characteristics of a single-stage centrifugal pump using a secondary noise source. *Proceedings 1st International Symposium on Pump Noise and Vibrations*, Clamart, France, pp. 175–182.

APPENDIX A: NOMENCLATURE

c	speed of sound
g	acceleration due to gravity
j	complex number
k	wave number
p^+	pressure wave in the direction of x positive
p^-	pressure wave in the direction of x negative

p_i pressure at the pump suction port
p_o pressure at the pump discharge port
p_s source pressure
p_s^+ source pressure in the direction of x positive
p_s^- source pressure in the direction of x negative
q_i acoustic velocity at the pump suction port
q_o acoustic velocity at the pump discharge port
q_s source acoustic velocity
t test loop temperature
x direction of pressure wave propagation
A pump diffuser throat area
H_{21} transfer function between pressure measurements
P total acoustic pressure field
R reflection coefficient
S pump scattering matrix
S_{ij} elements of the pump scattering matrix
T pump transmission matrix
T_{ij} elements of the pump transmission matrix
V pump volume
Z normalized acoustic impedance
Z_i normalized acoustic impedance at the pump suction port
Z_o normalized acoustic impedance at the pump discharge port
Z_p normalized pump acoustic impedance
ρ fluid density
ω circular frequency of pressure wave propagation
ω_s pump specific speed
ΔH pump head rate of change
ΔQ volumetric flow rate of change

APPENDIX B

Due to reflective characteristics of a piping system, the general one-dimensional pressure field can be expressed as

$$p(x, \omega) = p^+(0)(e^{-jkx} + Re^{jkx}), \tag{A1}$$

where $p^+(0)$ is the complex amplitude of the incident pressure wave and $R = re^{j2\sigma}$ is the complex reflection coefficient at any reflective surface. Now, the real and imaginary parts of the acoustic pressure $p(x, \omega)$ take the forms, respectively,

$$X = p^+(0)[\cos kx + r\cos(kx + 2\sigma)] \tag{A2}$$

and

$$Y = p^+(0)[-\sin kx + r\sin(kx + 2\sigma)]. \tag{A3}$$

Introducing a new variable $t = x + \sigma/k$, we can rearrange equations (A2) and (A3) as follows:

$$X = p^+(0)[\cos(kt - \sigma) + r\cos(kt + \sigma)] \tag{A4}$$

and

$$Y = p^+(0)[-\sin(kt - \sigma) + r\sin(kt + \sigma)]. \tag{A5}$$

After some algebra, equations (A4) and (A5) can be rewritten as

$$X = a\cos\sigma + b\sin\sigma \tag{A6}$$

and

$$Y = a\sin\sigma + b\cos\sigma \tag{A7}$$

where $a = p^+(0)(r+1)\cos kt$ and $b = p^+(0)(r-1)\sin kt$ represent the parametric equations of an ellipse. They yield

$$\left[\frac{a}{p^+(0)(1+r)}\right]^2 + \left[\frac{b}{p^+(0)(1-r)}\right]^2 = 1. \tag{A8}$$

It follows that equations (A6) and (A7), and thus equation (A1), describe an ellipse rotated by an angle σ relative to the reference coordinate system.